OPEN ACCESS
CellPress

Cell Reports
Article

Mitochondrial Pyruvate Carrier 2 Hypomorphism in Mice Leads to Defects in Glucose-Stimulated Insulin Secretion

Patrick A. Vigueira,[1,5] Kyle S. McCommis,[1,5] George G. Schweitzer,[1] Maria S. Remedi,[2] Kari T. Chambers,[1] Xiaorong Fu,[3] William G. McDonald,[4] Serena L. Cole,[4] Jerry R. Colca,[4] Rolf F. Kletzien,[4] Shawn C. Burgess,[3] and Brian N. Finck[1,*]

[1]Division of Geriatrics and Nutritional Sciences, Department of Medicine, Washington University School of Medicine, St. Louis, MO 63110, USA

[2]Department of Cell Biology and Physiology, Washington University School of Medicine, St. Louis, MO 63110, USA

[3]Advanced Imaging Research Center and Department of Pharmacology, University of Texas Southwestern Medical Center, Dallas, TX 75390, USA

[4]Metabolic Solutions Development Company, Kalamazoo, MI 49007, USA

[5]Co-first author

*Correspondence: bfinck@wustl.edu

http://dx.doi.org/10.1016/j.celrep.2014.05.017

This is an open access article under the CC BY license (http://creativecommons.org/licenses/by/3.0/).

SUMMARY

Carrier-facilitated pyruvate transport across the inner mitochondrial membrane plays an essential role in anabolic and catabolic intermediary metabolism. Mitochondrial pyruvate carrier 2 (Mpc2) is believed to be a component of the complex that facilitates mitochondrial pyruvate import. Complete MPC2 deficiency resulted in embryonic lethality in mice. However, a second mouse line expressing an N-terminal truncated MPC2 protein ($Mpc2^{\Delta 16}$) was viable but exhibited a reduced capacity for mitochondrial pyruvate oxidation. Metabolic studies demonstrated exaggerated blood lactate concentrations after pyruvate, glucose, or insulin challenge in $Mpc2^{\Delta 16}$ mice. Additionally, compared with wild-type controls, $Mpc2^{\Delta 16}$ mice exhibited normal insulin sensitivity but elevated blood glucose after bolus pyruvate or glucose injection. This was attributable to reduced glucose-stimulated insulin secretion and was corrected by sulfonylurea K_{ATP} channel inhibitor administration. Collectively, these data are consistent with a role for MPC2 in mitochondrial pyruvate import and suggest that Mpc2 deficiency results in defective pancreatic β cell glucose sensing.

INTRODUCTION

Pyruvate is an important three-carbon intermediate in energy metabolism and is a central substrate in carbohydrate, fat, and amino acid catabolic and anabolic pathways. Pyruvate is generated in the cytoplasm through glycolysis and subsequently is transported into the mitochondrion for oxidation or carboxylation, which is required for several critical metabolic processes (Figure 1A). For example, mitochondrial pyruvate carboxylation in the mitochondrial matrix results in the formation of oxaloacetate (an anaplerotic reaction), which is required for the biosynthesis of glucose via gluconeogenesis. Pyruvate entry into the mitochondrial matrix is also required for pyruvate oxidation, which is a prerequisite for the production of reducing equivalents in the tricarboxylic acid (TCA) cycle and production of citrate for de novo lipogenesis. Both pyruvate oxidation and carboxylation are critical for glucose-stimulated insulin secretion (GSIS) in pancreatic β cells (Jensen et al., 2008; Prentki et al., 2013; Sugden and Holness, 2011). Elevated blood glucose causes an increase in the intracellular ratio of ATP/ADP via increased mitochondrial pyruvate oxidation (Prentki et al., 2013; Sugden and Holness, 2011). ATP inhibits K_{ATP} channels, leading to depolarization, Ca^{2+} influx, and the release of insulin into the circulation (Huopio et al., 2002). Anaplerotic mitochondrial pyruvate metabolism activates pyruvate cycling pathways that alter NADPH, and regulates insulin secretion by inhibiting K_{ATP} channel activity as well (Jensen et al., 2008).

The existence of carrier-assisted transport of pyruvate across the inner mitochondrial membrane (IMM) was demonstrated in the 1970s (Halestrap, 1975; Halestrap and Denton, 1975; Papa et al., 1971). However, the proteins that facilitate pyruvate import into the mitochondrial matrix have only recently been identified (Bricker et al., 2012; Herzig et al., 2012). New evidence has emerged that the mitochondrial pyruvate carrier (MPC) is composed of two proteins, MPC1 and MPC2, which form a hetero-oligomeric complex in the IMM, and that both proteins are required for complex activity and stability (Bricker et al., 2012; Herzig et al., 2012). The MPC protein complex has been determined to be essential for mitochondrial pyruvate transport in *Drosophila* and yeast (Bricker et al., 2012; Herzig et al., 2012). In humans, mutations in MPC1 have been identified and associated with defects in mitochondrial pyruvate metabolism, lactic acidosis, hyperpyruvatemia, severe illness, and failure to thrive (Bricker et al., 2012; Brivet et al., 2003). Since its discovery, interest in the MPC complex as a drug target for cancer, neurological disorders, and metabolic diseases has been extremely

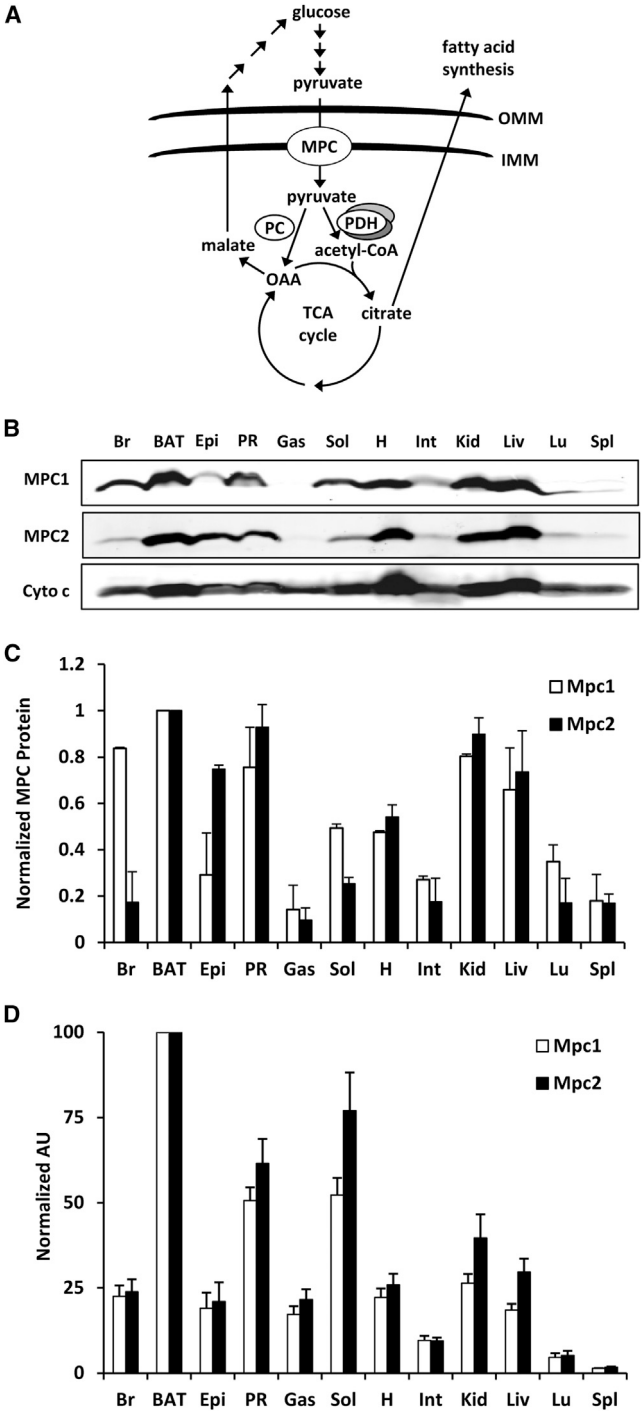

Figure 1. MPC Proteins Are Highly Expressed in Tissues with High Mitochondrial Content

(A) The schematic depicts an overview of mitochondrial pyruvate metabolism. OMM, outer mitochondrial membrane; IMM, inner mitochondrial membrane; PC, pyruvate carboxylase; PDH, pyruvate dehydrogenase; OAA, oxaloacetate; TCA, tricarboxylic acid.

(B) Western blot depicting expression of the indicated proteins in whole-cell lysates from various C57Bl/6 mouse tissues. Cytochrome *c* (cyto *c*) is shown to demonstrate mitochondrial abundance in the whole-cell lysates.

(C) Quantified densitometry of the western blot shown in (B). Data are presented as mean ± SEM (n = 3 separate animals).

(D) Expression pattern of Mpc1 and Mpc2 in C57Bl/6 mice as measured by qRT-PCR. Values are expressed as arbitrary units (AU) and presented as mean ± SEM (n = 5 separate animals). Br, brain; BAT, brown adipose tissue; Epi, epididymal adipose tissue; PR, perirenal adipose tissue; Gas, gastrocnemius; Sol, soleus; H, heart; Int, intestine; Kid, kidney; Liv, liver; Lu, lung; Spl, spleen.

high. Recent work suggests that insulin-sensitizing thiazolidinedione compounds bind the MPC complex (Colca et al., 2013) and modulate mitochondrial pyruvate oxidation (Divakaruni et al., 2013; Colca et al., 2013). Thus, a better understanding of MPC function has the potential to advance our knowledge about intermediary metabolism and impact drug discovery for current public health problems.

Herein, we report the generation and characterization of two MPC2-deficient mouse strains. Although complete MPC2 deficiency resulted in embryonic lethality, mice expressing a truncated, partially functional MPC2 protein were viable. Diminished pyruvate metabolism led to elevated blood lactate concentrations, particularly when mice were challenged with stimuli that increased glucose metabolism. The mutant mice also exhibited elevated blood glucose during glucose tolerance tests (GTTs) and pyruvate tolerance tests (PTTs) that was likely due to reduced GSIS. Additionally, glucose intolerance could be corrected by administration of K_{ATP} channel-inhibiting sulfonylurea drugs. These studies demonstrate the importance of mitochondrial pyruvate transport to glucose homeostasis in a mammalian system and support the continued exploration of mitochondrial function in complex metabolic diseases.

RESULTS

Tissue Expression of MPC Proteins

We first isolated various tissues from C57BL/6 mice to determine relative Mpc mRNA and MPC protein expression. We detected large variations in MPC protein (Figures 1B and 1C) and mRNA expression (Figure 1D), with the highest levels observed in tissues with greater mitochondrial abundance. Isolation and equal loading of mitochondrial lysate from these tissues somewhat normalized MPC1 and MPC2 protein expression (Figures S1A and S1B). However, MPC protein was still most abundant in highly oxidative tissues even when corrected for mitochondrial protein content.

Generation of Mpc2-Deficient Mice

We targeted the Mpc2 allele for deletion by using zinc-finger nuclease (ZFN) technology. The first line of mice harbored a deletion of 2 nt just downstream of the start codon (Figure S2A), resulting in a frameshift mutation and likely complete loss of protein product ($Mpc2^{-/-}$ mice). The mutation results in embryonic lethality in homozygous embryos. However, the number of heterozygous mice present at weaning was as predicted by Mendelian ratios (p = 0.717; Table S1), and these mice were overtly indistinguishable from their wild-type (WT) littermates. Lethality in homozygous embryos likely occurs between embryonic day 11 (E11) and E13, a period when robust mitochondrial biogenesis takes place (Cámara et al., 2011; Larsson et al.,

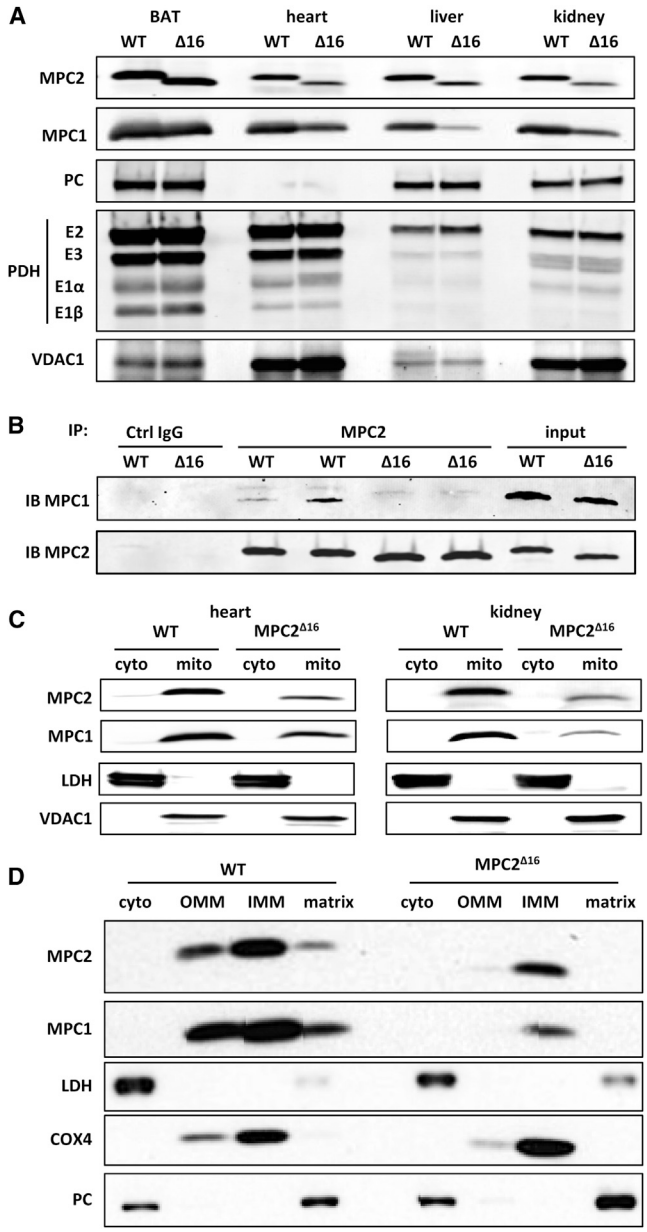

Figure 2. Generation of MPC2-Deficient Mice

(A) Western blot depicting the abundance of MPC1, MPC2, PC, and PDH complex protein in mitochondrial lysates of various tissues from Mpc2$^{\Delta 16}$ mice and WT controls. VDAC1 is used as a loading control.

(B) The ability of WT MPC2 and MPC2$^{\Delta 16}$ protein to coimmunoprecipitate MPC1 was tested by using an antibody against the C terminus of MPC2 and BAT mitochondrial lysates from WT and Mpc2$^{\Delta 16}$ mice. Negative control (irrelevant immunoglobulin G [IgG]) and input (nonprecipitated mitochondrial lysates) are also shown for comparison.

(C) Western blots for MPC1 and MPC2 after subcellular fractionation to separate cytosolic and mitochondrial fractions from WT and Mpc2$^{\Delta 16}$ mice are shown. LDH is used to demarcate the cytosolic fraction, and VDAC1 demarcates the mitochondrial fraction.

(D) Western blots after mitochondrial subfractionation to separate cytosolic, OMM, IMM, and matrix components by using liver from WT and Mpc2$^{\Delta 16}$ mice. LDH demarcates the cytosolic fraction, cytochrome *c* oxidase subunit 4 (Cox4) demarcates the IMM, and PC demarcates the matrix.

1998; Metodiev et al., 2009; Park et al., 2007). Timed mating studies yielded expected Mendelian ratios at embryonic days 10 and 11 ($p = 0.496$; Table S2), but no viable homozygote embryos at E13 (Table S3). Western blots of the tissues of heterozygous (Mpc2$^{+/-}$) mice demonstrated only a modest reduction in MPC2 and MPC1 protein compared with WT controls (Figure S2B). Pyruvate-driven oxygen consumption by isolated mitochondria from Mpc2$^{+/-}$ mice was not diminished compared with WT mitochondria (Figure S2C).

A second attempted knockout strategy resulted in the deletion of 20 nt including the original start codon for MPC2 translation. Despite the deletion, Mpc2 mRNA was expressed at normal levels (data not shown) and MPC2 protein translation proceeded from a second downstream start codon (Figure S2A). This resulted in a truncated protein that lacked the first 16 amino acids residues of the N terminus (MPC2$^{\Delta 16}$). Pups homozygous for the truncated allele were born at the expected Mendelian ratios ($p = 0.995$; Table S1) and were outwardly normal. The truncated protein, detected by western blotting with an antibody against the C terminus of MPC2, was less abundant than the WT protein in all tissues examined, except for brown adipose tissue (BAT; Figure 2A). The Mpc2$^{\Delta 16}$ mutation led to a marked reduction in the abundance of MPC1 protein, likely reflecting the maintenance of a stoichiometric ratio of MPC1 and MPC2 protein in the complex. Immunoprecipitation studies also indicated that the Mpc2$^{\Delta 16}$ mutant protein coimmunoprecipitated less MPC1 protein, suggesting that the interaction between the two proteins is significantly weakened by the loss of these 16 amino acids of MPC2 (Figure 2B). The abundance of the pyruvate dehydrogenase (PDH) complex and pyruvate carboxylase (PC) proteins was not altered in various tissues of the Mpc2$^{\Delta 16}$ mice, suggesting a lack of significant downstream alterations in pyruvate metabolic enzymes (Figure 2A). Western blotting of subfractionated kidney and heart demonstrated that the truncated Mpc2$^{\Delta 16}$ protein properly localized to mitochondria (Figure 2C) and specifically to the IMM in liver (Figure 2D).

Isolated Mpc2$^{\Delta 16}$ Mitochondria Have Reduced Oxygen Consumption

The Mpc2$^{\Delta 16}$ mice were healthy and appeared outwardly normal, suggesting that the MPC complex was at least partially functional. Plasma triglyceride was decreased and plasma ketone concentrations were increased in Mpc2$^{\Delta 16}$ mice compared with WT control mice (Table 1), suggesting an increased reliance on fat oxidation. Possibly consistent with a reduced capacity for mitochondrial pyruvate import, blood lactate concentrations were also significantly elevated (Table 1).

Therefore, we evaluated the effects of the MPC2 truncation on oxygen consumption in isolated mitochondria. We used heart and kidney tissue due to their high mitochondrial density and high MPC expression. Mpc2$^{\Delta 16}$ mitochondria from heart or kidney exhibited 25%–30% lower rates of pyruvate/malate-stimulated respiration in 2,4-dinitrophenol (DNP)-uncoupled conditions compared with WT controls (Figure 3A). Addition of methyl-pyruvate, a membrane-permeable pyruvate analog, rescued oxygen consumption to WT levels in Mpc2$^{\Delta 16}$ mitochondria. Additionally, maximal oxygen consumption rates in Mpc2$^{\Delta 16}$ mitochondria with glutamate/malate or

Table 1. Baseline Plasma Parameters

	WT	MPC2$^{\Delta16}$
Glucose (mg/dl)	125.1 ± 5.7	124.3 ± 5.1
Lactate (mmol/l)	1.6 ± 0.09	2.3 ± 0.11[a]
Insulin (ng/ml)	0.51 ± 0.09	0.34 ± 0.03
Triglyceride (mg/dl)	61.8 ± 2.2	54.8 ± 1.9[a]
NEFA (mmol/l)	0.58 ± 0.05	0.67 ± 0.05
Cholesterol (mg/dl)	65.3 ± 2.6	58.3 ± 3.7
Total ketones (mmol/l)	0.15 ± 0.01	0.25 ± 0.01[a]

[a]$p < 0.05$ versus WT. Data are expressed as mean ± SEM.

succinate/rotenone were unaltered compared with WT controls. Together, these data suggest a specific effect of the Mpc2$^{\Delta16}$ mutation on mitochondrial pyruvate oxidation.

Mitochondrial Membrane Potential Is Normal in Fibroblasts from Mpc2$^{\Delta16}$ Mice

Given the observed defect in pyruvate oxidation in Mpc2$^{\Delta16}$ tissues, we investigated whether these mitochondria displayed any sign of overt dysfunction by assessing the mitochondrial membrane potential ($\Delta\Psi_M$) in isolated adult fibroblasts of WT and Mpc2$^{\Delta16}$ mice. Tetramethylrhodamine, ethyl ester, perchlorate (TMRE) staining revealed no difference in $\Delta\Psi_M$, a comprehensive measure of overall mitochondrial function, in Mpc2$^{\Delta16}$ fibroblasts compared with WT controls (Figure 3B). The lack of effect on mitochondrial membrane potential was likely due to the small decrease in pyruvate-stimulated respiration and the maintained ability to metabolize other substrates.

Exercise Endurance Is Normal in MPC2$^{\Delta16}$ Mice

During exercise, significant quantities of pyruvate, which is interconverted to lactate, are generated via anaerobic glycolysis in skeletal muscle. Lactate, transported by the blood to the liver, is converted back to glucose that can again be used anaerobically as an energy source in muscle. This process, known as the Cori cycle (Katz and Tayek, 1999; Pilkis et al., 1988), depends on pyruvate import in liver mitochondria. Therefore, we challenged Mpc2$^{\Delta16}$ homozygote and Mpc2$^{+/-}$ mice using an acute endurance exercise bout of gradually increasing intensity until exhaustion (Figure 3C). The average blood glucose concentration of the Mpc2$^{\Delta16}$ mice was not different from that of WT controls in the 60 min after exercise (Figure 3C). However, the average blood lactate of the Mpc2$^{\Delta16}$ was approximately 2-fold higher compared with WT controls immediately after exercise and remained significantly elevated for 30 min postexercise (Figure 3C). Postexercise blood lactate and glucose concentrations were not different between Mpc2$^{+/-}$ and WT mice (Figure 3C). Despite the robust differences in blood lactate concentrations postexercise, we observed no significant differences in acute endurance exercise capacity among the genotypes (Figure 3C).

Elevated Blood Glucose and Lactate in Mpc2$^{\Delta16}$ Mice following Pyruvate Injection

To test the effects of the Mpc2 mutations on pyruvate disposal in vivo, we subjected Mpc2$^{\Delta16}$ homozygotes and

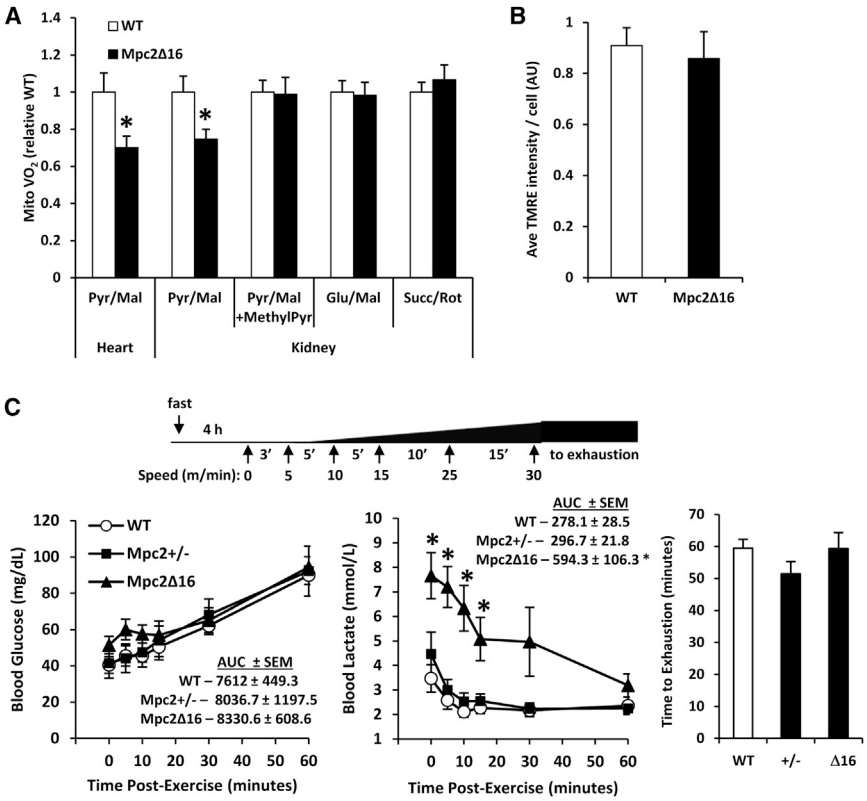

Figure 3. Mpc2$^{\Delta16}$ Mice Have a Diminished Capacity for Pyruvate Utilization, but Exercise Capacity Is Unimpaired

(A) DNP-stimulated rates of oxygen consumption by mitochondria isolated from heart or kidney of WT or Mpc2$^{\Delta16}$ mice in the presence of the indicated substrates (n = 8).

(B) TMRE staining of tail fibroblasts isolated from WT or Mpc2$^{\Delta16}$ mice (n = 8, separate experiments in duplicate).

(C) Schematic of the exercise protocol. Shown are blood glucose and blood lactate curves for WT, Mpc2$^{+/-}$, and Mpc2$^{\Delta16}$ mice following graduated-intensity exercise on a motor-driven treadmill (n = 6), and elapsed time until exhaustion for WT, Mpc2$^{+/-}$, and Mpc2$^{\Delta16}$ mice during graduated-intensity exercise (n = 6). Data are presented as mean ± SEM. *$p < 0.05$, Mpc2$^{\Delta16}$ versus WT.

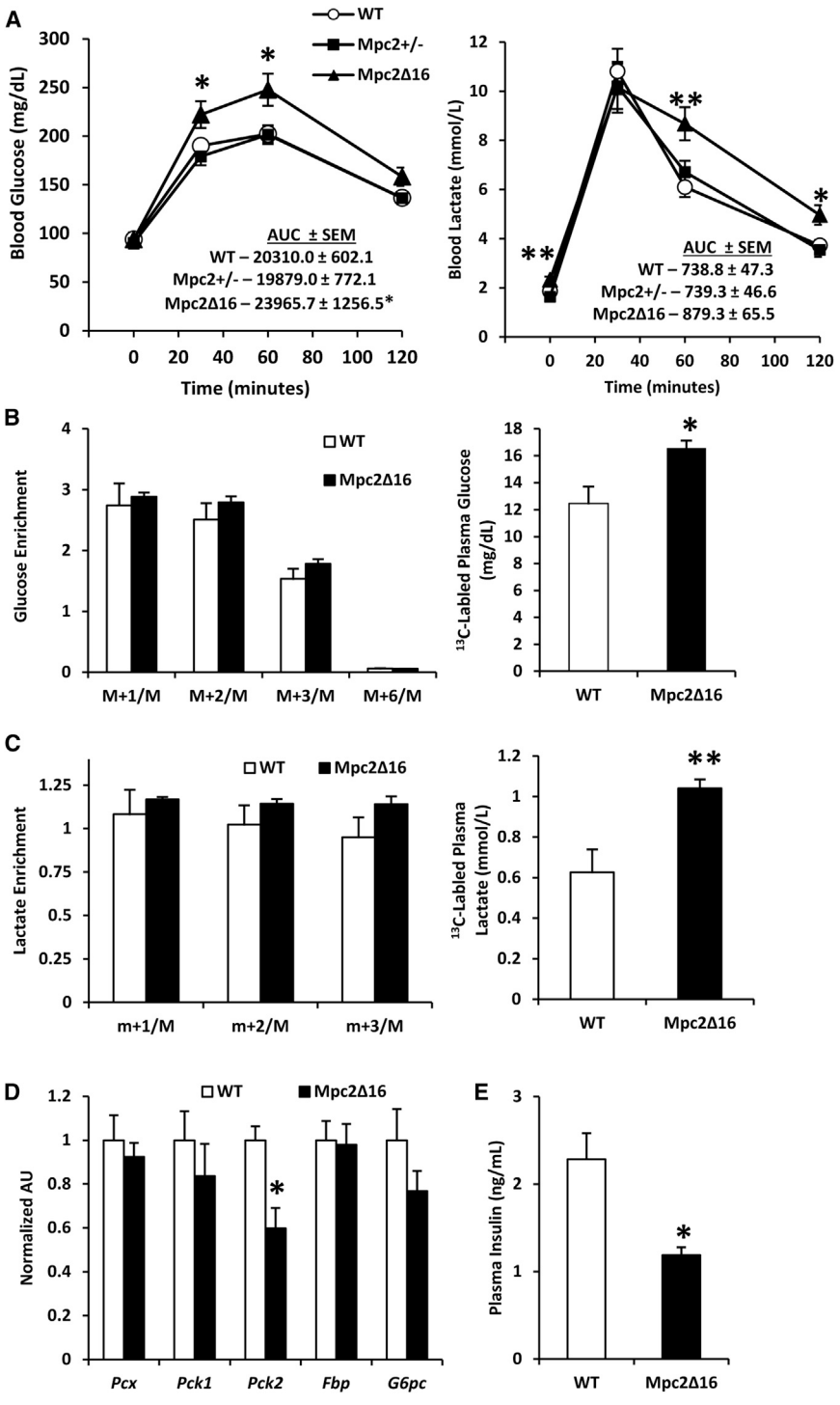

Figure 4. Mpc2$^{\Delta16}$ Mice Have Elevated Blood Glucose and Blood Lactate during a PTT, but Gluconeogenesis Remains Unimpaired

(A) Blood glucose and blood lactate curves for WT, Mpc2$^{+/-}$, and Mpc2$^{\Delta16}$ mice during i.p. PTT (n = 14).

(B) ^{13}C enrichment of plasma glucose isotopomers and total ^{13}C-labeled plasma glucose.

(C) ^{13}C enrichment of plasma lactate isotopomers and total ^{13}C-labeled plasma lactate (n = 7).

(D) Expression of liver gluconeogenesis enzymes.

(E) Plasma insulin 15 min after bolus pyruvate injection. Data are presented as mean ± SEM. *p < 0.05, **p < 0.01 Mpc2$^{\Delta16}$ versus WT.

Mpc2$^{+/-}$ mice to an intraperitoneal (i.p.) PTT. Following pyruvate injection, blood lactate increased 5-fold in all groups. However, the decline in blood lactate concentration was significantly slower in Mpc2$^{\Delta16}$ mice compared with WT controls (Figure 4A). Blood glucose and lactate levels were not different between Mpc2$^{+/-}$ and WT mice. Compared with WT mice, Mpc2$^{\Delta16}$ mice also exhibited a significantly greater blood glucose excursion (Figure 4A). These data are consistent with reduced pyruvate utilization resulting in elevated blood lactate concentrations.

To specifically evaluate the effect of the Mpc2$^{\Delta16}$ mutation on pyruvate gluconeogenesis and other intracellular pathways of pyruvate metabolism, we repeated the pyruvate challenge in Mpc2$^{\Delta16}$ mice with uniformly labeled [U-^{13}C]pyruvate. The mice were sacrificed, plasma and tissue were collected 60 min postinjection, and fractional ^{13}C enrichments were evaluated by mass spectrometry. There were no differences in hepatic oxaloacetate, malate, or fumarate concentrations or enrichments (Figure S3), indicating that liver mitochondrial pyruvate anaplerosis is intact in Mpc2$^{\Delta16}$ mice. Although the fractional enrichment of plasma glucose was unaffected by the Mpc2$^{\Delta16}$ mutation (Figure 4B), the plasma glucose concentration and therefore the total amount of ^{13}C-labeled plasma glucose were significantly elevated in Mpc2$^{\Delta16}$ mice versus WT mice (Figure 4B). These data suggest that the capacity for pyruvate-derived gluconeogenesis is intact in Mpc2$^{\Delta16}$ mice. Incorporation of ^{13}C-label into plasma lactate was not different between Mpc2$^{\Delta16}$ and WT control groups (Figure 4C). However, due to the increased lactate concentration in the blood, ^{13}C-labeled plasma lactate was significantly elevated in Mpc2$^{\Delta16}$ mice compared with WT controls (Figure 4C), consistent with decreased mitochondrial pyruvate metabolism in extrahepatic tissues. Additionally, expression of liver gluconeogenic enzymes was unaltered in Mpc2$^{\Delta16}$ mice, except

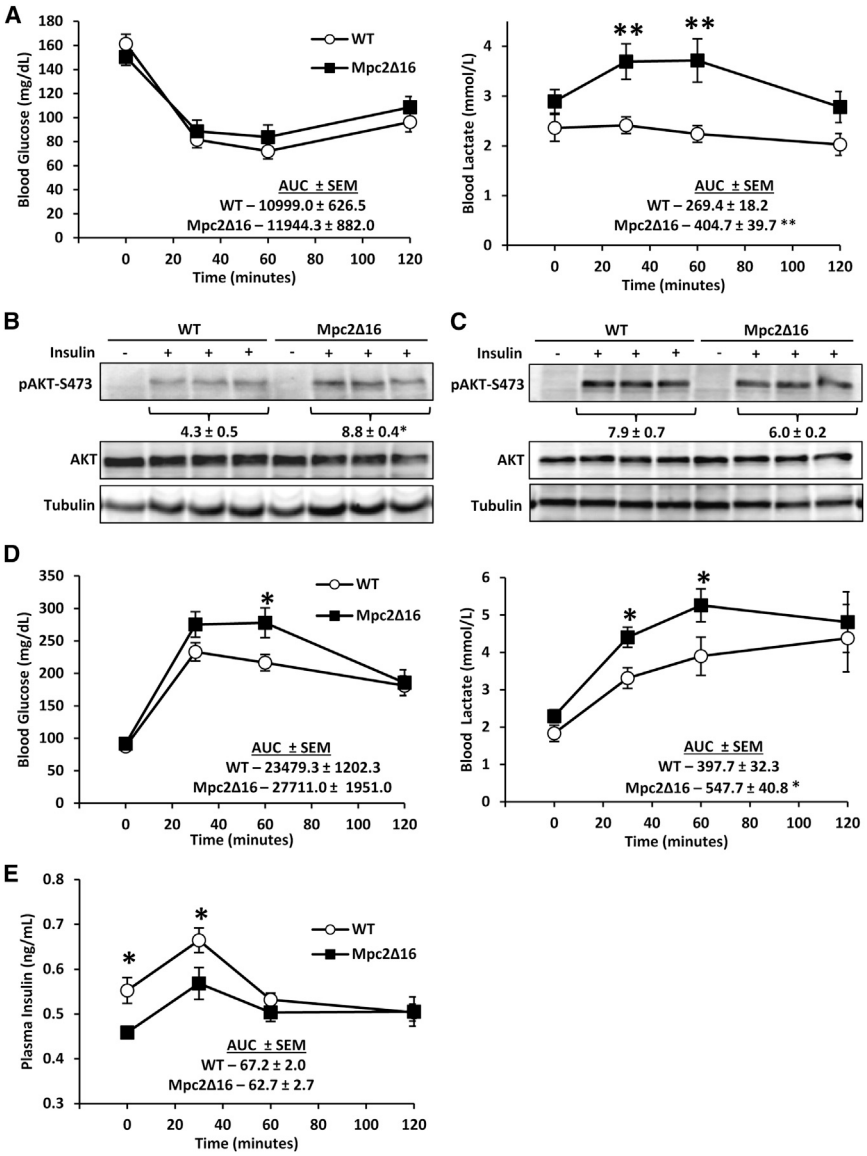

Figure 5. Mpc2$^{\Delta16}$ Mice Are Responsive to Insulin, but Are Glucose Intolerant and Hypoinsulinemic

(A) Blood glucose and blood lactate curves for WT and Mpc2$^{\Delta16}$ mice during i.p. ITT (n = 14). Data are presented as mean ± SEM. *p < 0.05, **p < 0.01 Mpc2$^{\Delta16}$ versus WT.

(B) Western blot and quantified densitometry of liver S473-AKT phosphorylation 15 min after insulin injection.

(C) Western blot and quantified densitometry of gastrocnemius S473-AKT phosphorylation 15 min after insulin injection.

(D) Blood glucose and blood lactate curves for WT and Mpc2$^{\Delta16}$ mice during an i.p. GTT (n = 15).

(E) Plasma insulin from blood collected during an i.p. glucose challenge (n = 9). Data are presented as mean ± SEM. *p < 0.05, **p < 0.01 Mpc2$^{\Delta16}$ versus WT.

that Pck2, which encodes the mitochondrial form of phosphoenolpyruvate carboxykinase, was significantly decreased (Figure 4D), suggesting that compensatory activation of these genes does not explain the intact gluconeogenic flux. Altogether, these data suggest that hepatic gluconeogenesis is not impaired in Mpc2$^{\Delta16}$ mice.

Mpc2$^{\Delta16}$ Mice Are Sensitive to Insulin, but Have Reduced Plasma Insulin and Elevated Blood Glucose

One possible explanation for the elevated blood glucose concentration in the PTT studies is that Mpc2$^{\Delta16}$ mice are insulin resistant. We conducted insulin tolerance tests (ITTs) to examine insulin effectiveness. Although blood lactate during the ITT was significantly elevated in Mpc2$^{\Delta16}$ mice compared with WT mice, blood glucose concentrations at all time points and the area under the curve (AUC) were not different, suggesting that insulin-stimulated glucose disposal is normal in Mpc2$^{\Delta16}$ mice (Figure 5A). Insulin-stimulated phosphorylation of Akt in liver was significantly enhanced (Figure 5B) and was unaltered in gastrocnemius muscle (Figure 5C) of Mpc2$^{\Delta16}$ mice compared with WT control mice. These data suggest that the Mpc2$^{\Delta16}$ mice have normal sensitivity to the effects of insulin.

In contrast, Mpc2$^{\Delta16}$ mice exhibited elevated blood lactate and trended toward a higher glucose AUC (p = 0.078) during an i.p. GTT (Figure 5D). Plasma insulin concentration was significantly lower in Mpc2$^{\Delta16}$ mice compared with WT controls at baseline and 30 min after glucose injection (Figure 5E), suggesting that glucose intolerance in Mpc2$^{\Delta16}$ mice was due to insufficient insulin secretion. Similarly, blood insulin concentration in Mpc2$^{\Delta16}$ mice compared with WT controls was also significantly lower 15 min after a bolus pyruvate injection (Figure 4E).

Impaired GSIS in Mpc2$^{\Delta16}$ Mice Is Corrected by Glibenclamide

The data obtained in GTT studies suggested a defect in GSIS by pancreatic islet β cells of Mpc2$^{\Delta16}$ mice. Both MPC1 and MPC2 are expressed in β cells, as demonstrated by colocalization with insulin in immunohistochemical staining of pancreatic sections (Figure 6A). Western blotting analyses confirmed that MPC1 and MPC2 proteins are expressed in isolated pancreatic islets and demonstrated that the expression of the MPC2$^{\Delta16}$ protein was markedly reduced compared with WT MPC2 (Figure 6B). Islet insulin content in Mpc2$^{\Delta16}$ mice was not different from that in WT controls (Figure 6C).

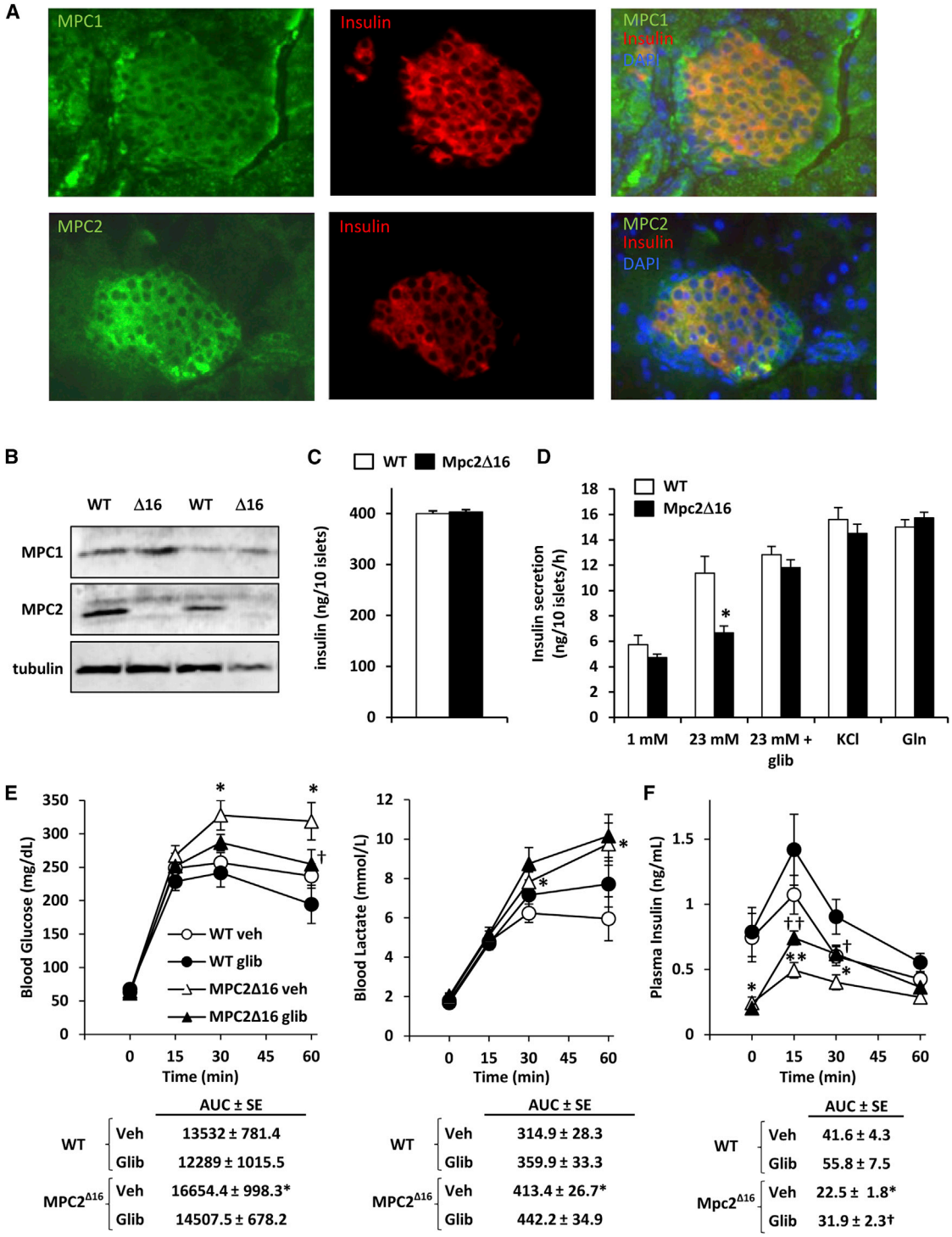

		AUC ± SE
WT	Veh	13532 ± 781.4
	Glib	12289 ± 1015.5
MPC2$^{\Delta16}$	Veh	16654.4 ± 998.3*
	Glib	14507.5 ± 678.2

		AUC ± SE
WT	Veh	314.9 ± 28.3
	Glib	359.9 ± 33.3
MPC2$^{\Delta16}$	Veh	413.4 ± 26.7*
	Glib	442.2 ± 34.9

		AUC ± SE
WT	Veh	41.6 ± 4.3
	Glib	55.8 ± 7.5
Mpc2$^{\Delta16}$	Veh	22.5 ± 1.8*
	Glib	31.9 ± 2.3†

Figure 6. Elevated Blood Glucose and Defective GSIS in Mpc2$^{\Delta16}$ Mice Are Corrected by Glibenclamide Treatment

(A) Images from immunofluorescent staining of pancreatic islets from C57Bl/6 mice with antibodies against MPC1 (green), MPC2 (green), or insulin (red) are shown.

(B) Western blot depicting the abundance of MPC2 and MPC1 protein using protein lysates from isolated islets from Mpc2$^{\Delta16}$ mice and WT controls.

(C) Insulin content of islets isolated from WT and Mpc2$^{\Delta16}$ mice (n = 6).

(D) Insulin secretion by isolated pancreatic islets from WT and Mpc2$^{\Delta16}$ mice in response to the indicated stimuli (n = 6).

(E) Blood glucose and blood lactate curves during an i.p. GTT for WT and Mpc2$^{\Delta16}$ mice treated with glibenclamide or saline vehicle (n = 11–13).

(F) Plasma insulin from blood collected during the experiment described in (E) (n = 11–13). Data are presented as mean ± SEM. *p < 0.05, **p < 0.01 Mpc2$^{\Delta16}$ versus WT.

We examined GSIS in isolated pancreatic islets from WT and Mpc2$^{\Delta 16}$ mice. Compared with WT islets, Mpc2$^{\Delta 16}$ islets exhibited reduced insulin secretion in response to 23 mM glucose (Figure 6D). β cell glucose sensing requires mitochondrial pyruvate metabolism, resulting in closure of the K_{ATP} channels (Huopio et al., 2002). We therefore examined the effects of glibenclamide, a sulfonylurea drug that inhibits K_{ATP} channel activity, on GSIS in Mpc2$^{\Delta 16}$ islets. As we hypothesized, the GSIS defect was rescued by the addition of glibenclamide to high-glucose media (Figure 6D). Additionally, Mpc2$^{\Delta 16}$ islets exhibited normal insulin secretion in response to KCl (Figure 6D). Supplementing high-glucose medium with glutamine, a metabolic substrate that does not require the MPC complex to enter the mitochondrion to be oxidized, also corrected the defect in GSIS (Figure 6D). These findings collectively suggest that the Mpc2$^{\Delta 16}$ insulin secretion defect is specific to stimulation by mitochondrial pyruvate metabolism rather than to a general deficiency in insulin production or defects in the insulin secretory machinery.

To confirm the relevance of these findings in vivo, we administered glibenclamide to Mpc2$^{\Delta 16}$ mice with a bolus of glucose in GTT studies. Vehicle-treated Mpc2$^{\Delta 16}$ mice exhibited elevated blood glucose concentrations compared with WT mice at 30 and 60 min postinjection, but blood glucose concentrations in Mpc2$^{\Delta 16}$ mice treated with glibenclamide were not different from those in vehicle-treated WT mice (Figure 6E). Administration of glibenclamide did not affect plasma lactate concentrations in mice of either genotype. Glibenclamide administration to Mpc2$^{\Delta 16}$ mice resulted in increased plasma insulin concentrations, which were reduced in Mpc2$^{\Delta 16}$ mice versus WT mice, at 15 and 30 min after injection (Figure 6F). These data further support the model in which whole-body Mpc2 deficiency leads to a defect in GSIS that is improved by K_{ATP} channel inhibition.

DISCUSSION

Carrier-mediated transport of pyruvate across the IMM is a critical step in intermediary metabolism, which is required for both anaplerotic and cataplerotic mitochondrial pyruvate metabolism. We found that complete loss of MPC2 led to embryonic lethality, but expression of a truncated MPC2 protein that exhibited hypomorphic activity was sufficient to support life. The most striking phenotypes of the Mpc2$^{\Delta 16}$ mice were elevated plasma lactate concentrations, particularly in the context of increased glucose concentrations, and a defect in β cell GSIS leading to relative glucose intolerance. These findings are consistent with a function for MPC2 in regulating mitochondrial pyruvate utilization and reveal important roles for MPC2 in regulating whole-body glucose homeostasis.

As mitochondrial pyruvate import is required in a number of critical metabolic pathways, it was not unexpected that complete ablation of Mpc2 resulted in embryonic lethality. Human mutations in MPC1 are associated with neonatal and juvenile mortality (Brivet et al., 2003). We were unable to recover viable Mpc2$^{-/-}$ embryos after E11, which is when mitochondrial function begins to play a larger role in embryonic metabolism (Cámara et al., 2011; Larsson et al., 1998; Metodiev et al., 2009; Park et al., 2007). Mpc2$^{+/-}$ mice exhibited only a modest reduction in MPC2 and MPC1 protein abundance, and were phenotypically indistinguishable from WT littermates in every parameter we examined. Our inability to detect a phenotype from the Mpc2$^{+/-}$ mice, even under conditions of metabolic challenge, likely highlights an excess transport capacity of the MPC complex.

We also serendipitously created a truncated mutant MPC2 protein as a consequence of the unpredictable results obtained by ZFN-mediated deletion. Although the Mpc2$^{\Delta 16}$ mutant has a nucleotide deletion larger than that of the Mpc2$^{-/-}$ mouse (20 bp versus 2 bp, respectively), it utilizes a downstream methionine as an alternative start site for translation of a truncated MPC2 protein. Because the original start codon is ablated by the 20 bp deletion but is intact in the 2 bp deletion, this allows an alternative ribosomal entry sequence to be enforced. This start codon may be less efficient or the resulting protein less stable, given that MPC2$^{\Delta 16}$ protein is less abundant than full-length MPC2. Most tissues in the Mpc2$^{\Delta 16}$ mice also had a significant reduction in abundance of the MPC1 protein. Previous work has shown that MPC1 and MPC2 must be coexpressed for proper assembly of the multimeric MPC complex, and that depletion of either protein leads to reduced abundance of the other (Bricker et al., 2012; Colca et al., 2013). It is likely that the reduced abundance of MPC1 in the Mpc2$^{\Delta 16}$ mice is due to the lower quantity of Mpc2$^{\Delta 16}$ compared with WT protein. A diminished or weakened protein-protein interaction between the two proteins is also a potential factor in the reduced complex stability, since less MPC1 was coimmunoprecipitated with MPC2$^{\Delta 16}$ compared with WT protein. However, the expression of MPC1 was only modestly affected by MPC2 truncation in BAT and islets, suggesting a tissue-specific regulation of MPC complex stability or the possible existence of homodimeric MPC protein complexes.

The truncated MPC2 protein is properly localized to the IMM and presumably, based on the phenotypes of the mutant mice, forms a transporter complex that is functionally hypomorphic. A number of mitochondrial carrier proteins of the IMM do not utilize canonical N-terminal mitochondrial localization sequences (Ferramosca and Zara, 2013; Pfanner and Geissler, 2001; Harbauer et al., 2014). Instead, these carriers utilize internal sequences that that have yet to be defined. Indeed, analysis by mitochondrial localization prediction programs, which predict mitochondrial targeting based on these canonical N-terminal localization sequences, did not produce a high-scoring prediction of mitochondrial localization for full-length or Δ16 MPC2 protein. However, the focus of this paper was not to define the targeting sequence, because that has been elusive for most mitochondrial proteins that lack the N-terminal canonical sequence.

Given that conversion of pyruvate into glucose by liver and kidney requires pyruvate to enter mitochondria for conversion to oxaloacetate, we expected that the Mpc2$^{\Delta 16}$ mice might be hypoglycemic in conditions requiring gluconeogenesis. Previous work using isolated liver preparations and a chemical inhibitor of MPC activity showed an acute inhibition of hepatic glucose output (Martin-Requero et al., 1986; Rognstad, 1983; Thomas and Halestrap, 1981). However, whether carrier-mediated pyruvate transport by MPC plays a significant role in controlling gluconeogenesis has been debated (Groen et al., 1983, 1986; Halestrap and Armston, 1984), and the hypomorphic function

of the MPC transport complex was not a limiting factor in the gluconeogenic capacity of Mpc2$^{\Delta 16}$ mice. Plasma ^{13}C-labeled glucose levels were actually increased in [U-^{13}C]PTT studies and Mpc2$^{\Delta 16}$ mice were not hypoglycemic following exhaustive exercise, suggesting that the Cori cycle was intact. The observation that gluconeogenesis was not impaired is not entirely unprecedented, given that previous studies have shown that an up to 85% reduction in phosphoenolpyruvate carboxykinase expression does not impact gluconeogenic flux (Burgess et al., 2007). Further work with other, more complete, liver-specific loss-of-function models will be needed to define the role that MPC complex proteins play in regulating hepatic gluconeogenesis.

Another interesting phenotype of the Mpc2$^{\Delta 16}$ mice was the hyperglycemia detected during PTT and GTT studies. Given that the insulin-stimulated decrease in blood glucose concentration was normal in ITT experiments and pyruvate metabolism is important for β cell glucose sensing (Lu et al., 2002; Prentki et al., 2013; Sugden and Holness, 2011), we suspected that insulin secretion might be defective. Indeed, plasma insulin concentration was diminished in Mpc2$^{\Delta 16}$ mice compared with WT mice during the GTT and PTT studies, and isolated islets from Mpc2$^{\Delta 16}$ mice exhibited an attenuated insulin secretion response following the administration of 23 mM glucose. Glucose sensing and GSIS require mitochondrial pyruvate oxidation and carboxylation. β cells express very little lactate dehydrogenase (LDH), and most of the pyruvate generated from glycolysis enters the mitochondrion for further metabolism (Malmgren et al., 2009; Schuit et al., 1997). Pyruvate carboxylation and oxidation inhibit ATP-sensitive potassium channels (K_{ATP}), depolarizing the β cell membrane, opening voltage-dependent calcium channels, and triggering the release of insulin into the circulation (Huopio et al., 2002). We found that the defects in insulin secretion by isolated islets and hypoinsulinemia/hyperglycemia in Mpc2$^{\Delta 16}$ mice were corrected by the sulfonylurea glibenclamide, which functions by binding and inhibiting the regulatory subunit of K_{ATP} channels. It is likely that glibenclamide is able to circumvent the reduced capacity of Mpc2$^{\Delta 16}$ mutants for mitochondrial pyruvate metabolism. The observation that glutamine, which relies upon its own IMM carrier (Indiveri et al., 1998), is able to stimulate insulin secretion in Mpc2$^{\Delta 16}$ islets also supports the notion of a specific defect in mitochondrial pyruvate metabolism. Consistent with these data, while this paper was in review, Patterson et al. (2014) used chemical inhibitors and small interfering RNA (siRNA) methods to suggest that MPC inhibition suppressed pyruvate metabolism and GSIS in isolated islets and β cell lines. Taken together, these studies demonstrate that the hypoinsulinemia of Mpc2$^{\Delta 16}$ mice is a specific defect in GSIS and not a broader indication of β cell dysfunction.

The molecular identification of MPC proteins has stimulated interest in targeting this complex for the treatment of many chronic disease states. Pharmacologic approaches to modulate the activity of the MPC complex could yield treatments for broad categories of obesity-related metabolic diseases, neurodegenerative conditions, and neoplastic diseases associated with impaired pyruvate metabolism (Constantin-Teodosiu, 2013; Schell and Rutter, 2013; Stacpoole, 2012). For example, the MPC complex has recently been identified as a binding site for the thiazolidinedione class of insulin sensitizers (Colca et al., 2013), which acutely modulate mitochondrial pyruvate oxidation (Divakaruni et al., 2013; Colca et al., 2013). The extent to which regulation of mitochondrial pyruvate import by thiazolidinediones affects insulin sensitization remains unclear, but could be addressed by MPC loss-of-function mouse models. Screens to identify small molecules that enhance, inhibit, or selectively modulate MPC activity may identify novel therapeutics with applicability to myriad chronic diseases.

EXPERIMENTAL PROCEDURES

Animal Studies

Unless otherwise noted, all experiments were conducted with 10- to 16-week-old female mice generated and maintained in a pure C57BL/6 background. All animal experiments were approved by the Animal Studies Committee of Washington University School of Medicine.

Generation of Mpc2-Deficient Mice

Mpc2 transgenic mice were generated by SAGE Labs using ZFN targeting technology (Geurts et al., 2009). Specifically, the target site sequence was TCCCTAGGCCGCCGCGATggcagCTGCCGGCGCCCGAGGCC (NCBI Ref Seq: NC_000067.5. Exon 1, nucleotides 199–203). ZFN pairs were microinjected into C57BL/6 zygotes and transferred to pseudopregnant C57BL/6 females at 0.5 days postcoitum.

Western Blotting

PAGE was performed on protein lysates utilizing Criterion precast gels (BioRad). Whole-cell lysates from tissue or cell culture were collected in HNET buffer containing protease and phosphatase inhibitors. For blots of mitochondrial lysates, mitochondria were obtained by differential centrifugation and solubilized in HNET buffer containing protease and phosphatase inhibitors. Blots on isolated pancreatic islets involved isolation of islets as described below, and 50 islets solubilized in 5× gel loading buffer per lane. For immunoprecipitation, 250 μg of BAT mitochondrial lysates was solubilized in lysis buffer containing 0.2% NP-40 and 10% glycerol. The lysates were precleared with 50 μl protein A beads and then incubated overnight with a rabbit MPC2 antibody (a gift from Michael Wolfgang). Protein A beads (50 μl) were then added 1 hr prior to immunoprecipitation. Liver mitochondrial fractionation was conducted as previously described (Benga et al., 1979) with slight modification. In brief, digitonin-treated mitochondria were centrifuged at 9,500 × *g*. The digitonin supernatants were centrifuged at 100,000 × *g* to isolate the outer membrane pellet (OMM) and the supernatant containing the inner membrane space. The digitonin pellet was loaded onto a discontinuous sucrose gradient to generate mitoplasts. The mitoplasts were treated with Lubrol WX and the IMM fractions were recovered from 100,000 × *g* discontinuous sucrose gradients. The antibodies utilized were β-Actin (Sigma-Aldrich), Akt (Cell Signaling Technology), pS473-Akt (CST), CoxIV (CST), cytochrome *c* (Abcam), LDH (Abcam), MPC1 and MPC2 (gifts from Michael Wolfgang), PC (Santa Cruz), PDH cocktail (Abcam), α-tubulin (Sigma), and voltage-dependent anion channel (VDAC; Abcam).

Quantitative PCR and RT-PCR

Total RNA was isolated using the RNAzol method (Tel-Test). Real-time PCR was performed using the ABI PRISM 7500 sequence detection system (Applied Biosystems) and the SYBR Green kit. Arbitrary units of target mRNA were corrected by measuring the levels of 36B4 RNA. The sequences of the oligonucleotides used in quantitative PCR (qPCR) analyses are listed in Table S4.

Measurement of Mitochondrial Respiration

Mitochondria from heart and kidney were isolated by differential centrifugation. High-resolution respirometry was conducted using a two-chamber Oxygraph O2k (Oroboros Instruments). We added 200 μg of mitochondria to

2 ml respiration buffer for each substrate trace. The respiratory substrates utilized were (concentration in mM) pyruvate (5)/malate (2), methyl-pyruvate (20)/pyruvate (5)/malate (2), glutamate (10)/malate (2), and succinate (10) + 1 μM rotenone. During pyruvate-stimulated respiration, 2 mM dichloroacetic acid was added to stimulate PDH (Divakaruni et al., 2013). After substrate addition and measurement of basal respiration, maximally stimulated, uncoupled respiration was measured by addition of 2 μg/ml oligomycin and 10 μM DNP.

Isolation of Adult Murine Fibroblasts and Measurement of Mitochondrial Membrane Potential

Isolation of primary adult murine fibroblasts from tail clip was performed as previously described (Huss et al., 2004). Fibroblasts from WT and $Mpc2^{\Delta 16}$ mice were cultured in high-glucose Dulbecco's modified Eagle's medium supplemented with 20% fetal bovine serum. Cells were plated onto four-well glass chamber slides (Lab-Tek II) at a density of 30,000 cells/well and incubated overnight. The cells were then stained with 100 nM TMRE in Hank's balanced salt solution (HBSS) for 30 min, washed with HBSS, and imaged on an inverted fluorescence microscope (Nikon Instruments). The average TMRE fluorescence per cell was determined with ImageJ (NIH).

Acute Exercise Protocol

WT, $Mpc2^{\Delta 16}$, and $Mpc2^{+/-}$ mice performed a single bout of treadmill exercise to exhaustion. The mice were fasted for 4 hr prior to the exercise session. Following a 3 min familiarization period on the treadmill, the exercise protocol consisted of graduated intensity running at 5 m/min for 5 min, 10 m/min for 5 min, 15 m/min for 10 min, 25 m/min for 15 min, and 30 m/min until the mouse fatigued. The mice were encouraged to run with a mild electric stimulus (20 V) positioned at the end of the treadmill and were determined to be exhausted by their refusal to remain on the treadmill belt for 5 s. Postexercise blood glucose and lactate levels were determined at 0, 5, 10, 20, 30, 60, and 120 min after exhaustion.

Measurement of Baseline Plasma Parameters

Mice were fasted for 4 hr and tail blood glucose and lactate concentrations were determined using a One-Touch Ultra glucometer (LifeScan) and a Lactate Plus lactate meter (Nova Biomedical), respectively. Blood samples for plasma analyses were collected by mandibular bleeding. Plasma insulin was measured with an ultrasensitive ELISA (Crystal Chem). Plasma triglyceride and cholesterol concentrations were measured by Infinity assay kits (Thermo Fisher Scientific). Nonesterified fatty acids (NEFAs) and total ketone concentrations were measured using enzymatic assays (Wako Diagnostics).

GTT, PTT, and ITT

For the GTT and PTT, mice were fasted overnight for 16 hr and housed on aspen chip bedding. The mice were injected i.p. with 1 g/kg body weight glucose or with 2 g/kg body weight Na-pyruvate dissolved in sterile physiological saline. For the ITT, mice were fasted for 6 hr and injected i.p. with 0.75 U/kg body weight insulin. Tail blood glucose and lactate concentrations were determined at 0, 30, 60, and 120 min after challenge as described above. The total AUC was calculated using the trapezoidal rule. Blood samples for plasma insulin quantification were collected by mandibular bleeding as described above. A subset of mice were injected i.p. with 2 g/kg body weight Na-pyruvate and sacrificed at 15 min to determine plasma insulin concentrations during pyruvate challenge. To examine insulin-stimulated protein phosphorylation, a subset of mice were injected i.p. with 10 mU/g body weight human insulin 15 min before sacrifice to collect liver and muscle tissue.

The glibenclamide rescue studies were conducted in the context of a standard GTT, with sample time points adjusted to 0, 15, 30, and 60 min after challenge. Glibenclamide was administered at 0.1 mg/kg body weight in a glucose solution that contained 0.1% DMSO. Blood was collected at each time point by means of mandibular bleeding as described above.

^{13}C-Labeled Pyruvate Studies

Pyruvate labeling studies were conducted as previously described (Méndez-Lucas et al., 2013). Briefly, mice were fasted for 16 hr and injected i.p. with 2 g pyruvate per kg body weight with a 10% enrichment of uniformly labeled [U-^{13}C3]Na-pyruvate (Cambridge Isotope Laboratories). The mice were sacrificed at 60 min postinjection and plasma was analyzed by gas chromatography-mass spectrometry as previously described (Sunny and Bequette, 2010).

Pancreas Immunohistochemistry

Protein expression of MPCs in pancreatic islets was determined in paraffin-embedded pancreatic sections from WT mice cut onto glass slides. The slides were rehydrated, permeabilized with trypsin, blocked in 1% BSA, and probed with guinea pig anti-insulin (Abcam) and either rabbit anti-MPC1 or rabbit anti-MPC2 (gifts from Michael Wolfgang). All antibodies were diluted 1:200 in buffer containing 1% BSA and incubations were conducted overnight. The sections were then washed three times for 5 min in PBS and probed with 1:1,000 donkey anti-rabbit green or 1:1,000 donkey anti-guinea pig red Alexa Fluor secondary antibodies (Invitrogen) for 2 hr. The slides were again washed three times for 5 min in PBS, mounted with Vectashield + DAPI, and imaged on an epifluorescence microscope (Nikon Instruments).

Islet Isolation and Insulin Release Experiments

Islet isolation and insulin release studies were performed as previously described (Remedi et al., 2004). Briefly, after the mice were euthanized, the pancreases were removed and injected with HBSS (Sigma) containing collagenase (0.5 mg/ml, pH 7.4). They were digested for 4 min at 37°C, and the islets were isolated by hand. Following overnight incubation in 3 mM glucose CMRL-1066 medium, islets (10 per well in 12-well plates) were incubated for 60 min at 37°C in CMRL-1066 + 1 mM glucose, 23 mM glucose, 23 mM glucose + 1 μM glibenclamide, 1 mM + 30 mM KCl, or 23 mM glucose + 10 mM glutamine, as indicated. After the incubation period, the medium was removed and assayed for insulin release. Experiments were repeated in triplicate. To estimate the islet insulin content, groups of ten islets were disrupted by ethanol-HCl extraction and sonicated on ice. Insulin secretion and content were measured using a rat insulin radioimmunoassay (Millipore) according to the manufacturer's instructions.

Statistical Analyses

Statistical comparisons were made using ANOVA, chi-square test, or t test. All data are presented as means ± SEM, with a statistically significant difference defined as $p < 0.05$.

SUPPLEMENTAL INFORMATION

Supplemental Information includes three figures and four tables and can be found with this article online at http://dx.doi.org/10.1016/j.celrep.2014.05.017.

AUTHOR CONTRIBUTIONS

P.A.V. and K.S.M. performed experiments, analyzed data, generated figures, and wrote the manuscript. G.G.S. and M.S.R. performed experiments, analyzed data, generated figures, and wrote portions of the manuscript. K.T.C. and X.F. performed experiments and edited the manuscript. W.G.M. performed experiments, analyzed data, generated figures, and wrote portions of the manuscript. S.L.C. performed experiments and edited the manuscript. J.R.C. and R.F.K. analyzed data and edited the manuscript. S.C.B. and B.N.F. analyzed data and wrote portions of the manuscript.

ACKNOWLEDGMENTS

This work was supported by NIH grants R01 DK078187 and R42 AA021228. A grant from the Barnes Jewish Hospital Foundation and the core services of the Digestive Diseases Research Core Center (P30 DK52574), Diabetes Research Center (P30 DK20579), and the Nutrition Obesity Research Center (P30 DK56341) at Washington University School of Medicine also supported this work. S.C.B. is supported by NIH grants P01 DK078184 and P01 DK058398, and the Robert A. Welch Foundation (I-1804-01). P.A.V. and K.S.M are Diabetes Research Postdoctoral Training Program fellows (T32 DK007296). G.G.S. is supported by NIH training grant T32 HL007275, and K.T.C. is an American Liver Foundation Liver Scholar. S.L.C., W.G.M., J.R.C., and R.F.K.

are founders, employees, and significant stockholders of Metabolic Solutions Development Company.

Received: February 3, 2014
Revised: April 15, 2014
Accepted: May 8, 2014
Published: June 5, 2014

REFERENCES

Benga, G., Hodarnau, A., Tilinca, R., Porutiu, D., Dancea, S., Pop, V., and Wrigglesworth, J. (1979). Fractionation of human liver mitochondria: enzymic and morphological characterization of the inner and outer membranes as compared with rat liver mitochondria. J. Cell Sci. *35*, 417–429.

Bricker, D.K., Taylor, E.B., Schell, J.C., Orsak, T., Boutron, A., Chen, Y.-C., Cox, J.E., Cardon, C.M., Van Vranken, J.G., Dephoure, N., et al. (2012). A mitochondrial pyruvate carrier required for pyruvate uptake in yeast, Drosophila, and humans. Science *337*, 96–100.

Brivet, M., Garcia-Cazorla, A., Lyonnet, S., Dumez, Y., Nassogne, M.C., Slama, A., Boutron, A., Touati, G., Legrand, A., and Saudubray, J.M. (2003). Impaired mitochondrial pyruvate importation in a patient and a fetus at risk. Mol. Genet. Metab. *78*, 186–192.

Burgess, S.C., He, T., Yan, Z., Lindner, J., Sherry, A.D., Malloy, C.R., Browning, J.D., and Magnuson, M.A. (2007). Cytosolic phosphoenolpyruvate carboxykinase does not solely control the rate of hepatic gluconeogenesis in the intact mouse liver. Cell Metab. *5*, 313–320.

Cámara, Y., Asin-Cayuela, J., Park, C.B., Metodiev, M.D., Shi, Y., Ruzzenente, B., Kukat, C., Habermann, B., Wibom, R., Hultenby, K., et al. (2011). MTERF4 regulates translation by targeting the methyltransferase NSUN4 to the mammalian mitochondrial ribosome. Cell Metab. *13*, 527–539.

Colca, J.R., McDonald, W.G., Cavey, G.S., Cole, S.L., Holewa, D.D., Brightwell-Conrad, A.S., Wolfe, C.L., Wheeler, J.S., Coulter, K.R., Kilkuskie, P.M., et al. (2013). Identification of a mitochondrial target of thiazolidinedione insulin sensitizers (mTOT)—relationship to newly identified mitochondrial pyruvate carrier proteins. PLoS ONE *8*, e61551.

Constantin-Teodosiu, D. (2013). Regulation of muscle pyruvate dehydrogenase complex in insulin resistance: effects of exercise and dichloroacetate. Diabetes Metab. J. *37*, 301–314.

Divakaruni, A.S., Wiley, S.E., Rogers, G.W., Andreyev, A.Y., Petrosyan, S., Loviscach, M., Wall, E.A., Yadava, N., Heuck, A.P., Ferrick, D.A., et al. (2013). Thiazolidinediones are acute, specific inhibitors of the mitochondrial pyruvate carrier. Proc. Natl. Acad. Sci. USA *110*, 5422–5427.

Ferramosca, A., and Zara, V. (2013). Biogenesis of mitochondrial carrier proteins: molecular mechanisms of import into mitochondria. Biochim. Biophys. Acta *1833*, 494–502.

Geurts, A.M., Cost, G.J., Freyvert, Y., Zeitler, B., Miller, J.C., Choi, V.M., Jenkins, S.S., Wood, A., Cui, X., Meng, X., et al. (2009). Knockout rats via embryo microinjection of zinc-finger nucleases. Science *325*, 433.

Groen, A.K., Vervoorn, R.C., Van der Meer, R., and Tager, J.M. (1983). Control of gluconeogenesis in rat liver cells. I. Kinetics of the individual enzymes and the effect of glucagon. J. Biol. Chem. *258*, 14346–14353.

Groen, A.K., van Roermund, C.W., Vervoorn, R.C., and Tager, J.M. (1986). Control of gluconeogenesis in rat liver cells. Flux control coefficients of the enzymes in the gluconeogenic pathway in the absence and presence of glucagon. Biochem. J. *237*, 379–389.

Halestrap, A.P. (1975). The mitochondrial pyruvate carrier. Kinetics and specificity for substrates and inhibitors. Biochem. J. *148*, 85–96.

Halestrap, A.P., and Denton, R.M. (1975). The specificity and metabolic implications of the inhibition of pyruvate transport in isolated mitochondria and intact tissue preparations by alpha-Cyano-4-hydroxycinnamate and related compounds. Biochem. J. *148*, 97–106.

Halestrap, A.P., and Armston, A.E. (1984). A re-evaluation of the role of mitochondrial pyruvate transport in the hormonal control of rat liver mitochondrial pyruvate metabolism. Biochem. J. *223*, 677–685.

Harbauer, A.B., Zahedi, R.P., Sickmann, A., Pfanner, N., and Meisinger, C. (2014). The protein import machinery of mitochondria-a regulatory hub in metabolism, stress, and disease. Cell Metab. *19*, 357–372.

Herzig, S., Raemy, E., Montessuit, S., Veuthey, J.-L., Zamboni, N., Westermann, B., Kunji, E.R.S., and Martinou, J.-C. (2012). Identification and functional expression of the mitochondrial pyruvate carrier. Science *337*, 93–96.

Huopio, H., Shyng, S.-L., Otonkoski, T., and Nichols, C.G. (2002). K(ATP) channels and insulin secretion disorders. Am. J. Physiol. Endocrinol. Metab. *283*, E207–E216.

Huss, J.M., Torra, I.P., Staels, B., Giguère, V., and Kelly, D.P. (2004). Estrogen-related receptor α directs peroxisome proliferator-activated receptor α signaling in the transcriptional control of energy metabolism in cardiac and skeletal muscle. Mol. Cell. Biol. *24*, 9079–9091.

Indiveri, C., Abruzzo, G., Stipani, I., and Palmieri, F. (1998). Identification and purification of the reconstitutively active glutamine carrier from rat kidney mitochondria. Biochem. J. *333*, 285–290.

Jensen, M.V., Joseph, J.W., Ronnebaum, S.M., Burgess, S.C., Sherry, A.D., and Newgard, C.B. (2008). Metabolic cycling in control of glucose-stimulated insulin secretion. Am. J. Physiol. Endocrinol. Metab. *295*, E1287–1297.

Katz, J., and Tayek, J.A. (1999). Recycling of glucose and determination of the Cori Cycle and gluconeogenesis. Am. J. Physiol. *277*, E401–E407.

Larsson, N.G., Wang, J., Wilhelmsson, H., Oldfors, A., Rustin, P., Lewandoski, M., Barsh, G.S., and Clayton, D.A. (1998). Mitochondrial transcription factor A is necessary for mtDNA maintenance and embryogenesis in mice. Nat. Genet. *18*, 231–236.

Lu, D., Mulder, H., Zhao, P., Burgess, S.C., Jensen, M.V., Kamzolova, S., Newgard, C.B., and Sherry, A.D. (2002). 13C NMR isotopomer analysis reveals a connection between pyruvate cycling and glucose-stimulated insulin secretion (GSIS). Proc. Natl. Acad. Sci. USA *99*, 2708–2713.

Malmgren, S., Nicholls, D.G., Taneera, J., Bacos, K., Koeck, T., Tamaddon, A., Wibom, R., Groop, L., Ling, C., Mulder, H., and Sharoyko, V.V. (2009). Tight coupling between glucose and mitochondrial metabolism in clonal beta-cells is required for robust insulin secretion. J. Biol. Chem. *284*, 32395–32404.

Martin-Requero, A., Ayuso, M.S., and Parrilla, R. (1986). Rate-limiting steps for hepatic gluconeogenesis. Mechanism of oxamate inhibition of mitochondrial pyruvate metabolism. J. Biol. Chem. *261*, 13973–13978.

Méndez-Lucas, A., Duarte, J.A.G., Sunny, N.E., Satapati, S., He, T., Fu, X., Bermúdez, J., Burgess, S.C., and Perales, J.C. (2013). PEPCK-M expression in mouse liver potentiates, not replaces, PEPCK-C mediated gluconeogenesis. J. Hepatol. *59*, 105–113.

Metodiev, M.D., Lesko, N., Park, C.B., Cámara, Y., Shi, Y., Wibom, R., Hultenby, K., Gustafsson, C.M., and Larsson, N.-G. (2009). Methylation of 12S rRNA is necessary for in vivo stability of the small subunit of the mammalian mitochondrial ribosome. Cell Metab. *9*, 386–397.

Papa, S., Francavilla, A., Paradies, G., and Meduri, B. (1971). The transport of pyruvate in rat liver mitochondria. FEBS Lett. *12*, 285–288.

Park, C.B., Asin-Cayuela, J., Cámara, Y., Shi, Y., Pellegrini, M., Gaspari, M., Wibom, R., Hultenby, K., Erdjument-Bromage, H., Tempst, P., et al. (2007). MTERF3 is a negative regulator of mammalian mtDNA transcription. Cell *130*, 273–285.

Patterson, J.N., Cousteils, K., Lou, J.W., Manning Fox, J.E., Macdonald, P.E., and Joseph, J.W. (2014). Mitochondrial metabolism of pyruvate is essential for regulating glucose-stimulated insulin secretion. J. Biol. Chem. *289*, 13335–13346.

Pfanner, N., and Geissler, A. (2001). Versatility of the mitochondrial protein import machinery. Nat. Rev. Mol. Cell Biol. *2*, 339–349.

Pilkis, S.J., el-Maghrabi, M.R., and Claus, T.H. (1988). Hormonal regulation of hepatic gluconeogenesis and glycolysis. Annu. Rev. Biochem. *57*, 755–783.

Prentki, M., Matschinsky, F.M., and Madiraju, S.R.M. (2013). Metabolic signaling in fuel-induced insulin secretion. Cell Metab. *18*, 162–185.

Remedi, M.S., Koster, J.C., Markova, K., Seino, S., Miki, T., Patton, B.L., McDaniel, M.L., and Nichols, C.G. (2004). Diet-induced glucose intolerance in mice with decreased beta-cell ATP-sensitive K+ channels. Diabetes *53*, 3159–3167.

Rognstad, R. (1983). The role of mitochondrial pyruvate transport in the control of lactate gluconeogenesis. Int. J. Biochem. *15*, 1417–1421.

Schell, J.C., and Rutter, J. (2013). The long and winding road to the mitochondrial pyruvate carrier. Cancer Metab. *1*, 6.

Schuit, F., De Vos, A., Farfari, S., Moens, K., Pipeleers, D., Brun, T., and Prentki, M. (1997). Metabolic fate of glucose in purified islet cells. Glucose-regulated anaplerosis in beta cells. J. Biol. Chem. *272*, 18572–18579.

Stacpoole, P.W. (2012). The pyruvate dehydrogenase complex as a therapeutic target for age-related diseases. Aging Cell *11*, 371–377.

Sugden, M.C., and Holness, M.J. (2011). The pyruvate carboxylase-pyruvate dehydrogenase axis in islet pyruvate metabolism: Going round in circles? Islets *3*, 302–319.

Sunny, N.E., and Bequette, B.J. (2010). Gluconeogenesis differs in developing chick embryos derived from small compared with typical size broiler breeder eggs. J. Anim. Sci. *88*, 912–921.

Thomas, A.P., and Halestrap, A.P. (1981). The rôle of mitochondrial pyruvate transport in the stimulation by glucagon and phenylephrine of gluconeogenesis from L-lactate in isolated rat hepatocytes. Biochem. J. *198*, 551–560.